ACS OMEGA

Open Access

http://pubs.acs.org/journal/acsodf

Article

Antimicrobial Activity against *Fusarium oxysporum* f. sp. dianthi of TiO_2/ZnO Thin Films under UV Irradiation: Experimental and Theoretical Study

Cesar Quiñones, Martha Posada, Angie Hormiga, Julian Peña, Carlos Diaz-Uribe, William Vallejo,* Amner Muñoz-Acevedo, Vanesa Roa, Eduardo Schott, and Ximena Zarate

Cite This: *ACS Omega* 2024, 9, 31546−31555

Read Online

ACCESS | Metrics & More | Article Recommendations | Supporting Information

ABSTRACT: We deposited bare TiO_2 and TiO_2/ZnO thin films to study their antimicrobial capacity against *Fusarium oxysporum* f. sp. dianthi. The deposit of TiO_2 was performed by spin coating and the ZnO thin films were deposited onto the TiO_2 surface by plasma-assisted reactive evaporation technique. The characterization of the compounds was carried out by scanning electron microscopy (SEM) and powder X-ray diffraction techniques. Furthermore, density functional theory (DFT) and time-dependent DFT (TDDFT) calculations were performed to support the observed experimental results. Thus, the removal of methylene blue (MB) by adsorption and posterior photocatalytic degradation was studied. Adsorption kinetic results showed that TiO_2/ZnO thin films were more efficient in MB removal than bare TiO_2 thin films, and the pseudo-second-order model was suitable to describe the experimental results for TiO_2/ZnO (q_e = 12.9 mg/g; k_2 = 0.14 g/mg/min) and TiO_2 thin films (q_e = 12.0 mg/g; k_2 = 0.13 g/mg/min). Photocatalytic results under UV irradiation showed that TiO_2 thin films reached 10.9% of MB photodegradation ($k = 1.0 \times 10^{-3}$ min^{-1}), whereas TiO_2/ZnO thin films reached 20.6% of MB photodegradation ($k = 3.9 \times 10^{-3}$ min^{-1}). Both thin films reduced the photocatalytic efficiency by less than 3% after 4 photocatalytic tests. DFT study showed that the highest occupied molecular orbital−lowest unoccupied molecular orbital (HOMO−LUMO) energy gap decreases for the mixed nanoparticle system, showing its increased reactivity. Furthermore, the chemical hardness shows a lower value for the mixed system, whereas the electrophilicity index shows the biggest value, supporting the larger reactivity for the mixed nanoparticle system. Finally, the antimicrobial activity against *F. oxysporum* f. sp. dianthi showed that bare TiO_2 reached a growth reduction of 68% while TiO_2/ZnO reached a growth reduction of 90% after 250 min of UV irradiation.

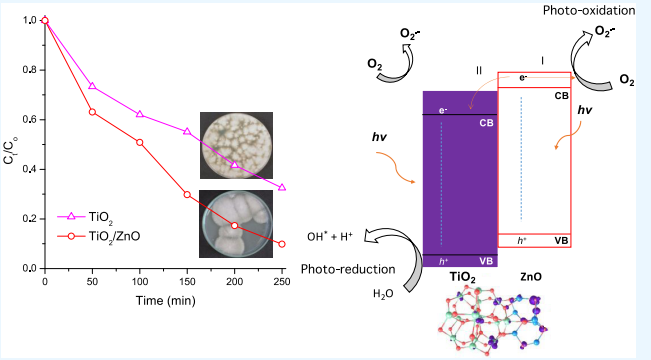

1. INTRODUCTION

The advanced oxidation process (AOP) is a group of physicochemical techniques (e.g., O_3/UV, O_3/H_2O_2, UV/H_2O_2, Fenton, heterogeneous catalysis, electrochemical oxidation, photolysis, radiolysis, cavitation, and γ radiation)[1] that has proven its effectiveness for partial or complete mineralization of different pollutants. Heterogeneous photocatalysis is commonly implemented in various processes to remove organic pollutants present in aqueous and gaseous media. Thus, heterogeneous photocatalysis is an AOP that has proven its effectiveness in treating polluted effluents, such as air and water. This process presents advantages like a wide range of working pH and the easy recovery of the catalysis (e.g., compared with the Fenton process).[2] Heterogeneous photocatalysis allows the removal of different organic pollutants (e.g., phenols, chlorinated organic compounds, pharmaceuticals, pesticides,[3−5] dyes,[6] phenolic,[7] organic compounds,[8] and antibiotics,[9] among others). Furthermore, heterogeneous photocatalysis is considered as a "green process" for water treatment.[10] Currently, microbial contamination has become an important public issue because different microorganisms affect the environment and human life.[11] The antimicrobial resistance of different microorganisms (e.g., parasites, bacteria, and fungi) is a global issue. Developing strategies to solve microbial resistance is a requirement for sustainable progress. Specifically in the agriculture field, losses associated with pesticide resistance were estimated at 1.5 billion USD/year, only in the United States.[12] The *Fusarium oxysporum* f. sp. dianthi (FOFspd) is a complex and adaptative species of Eumycota fungi species. The Fusarium genus fungi

Received: February 12, 2024
Revised: March 17, 2024
Accepted: April 25, 2024
Published: July 10, 2024

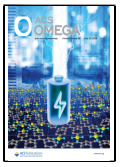

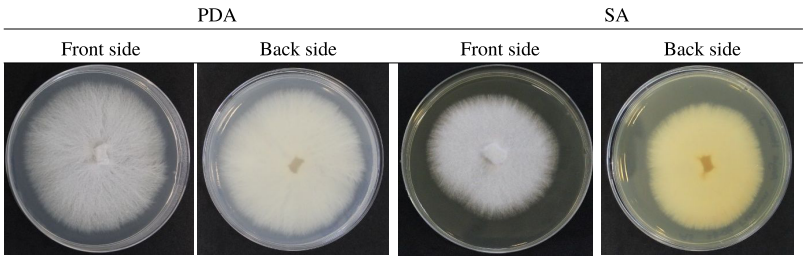

Figure 1. FOFspd in the PDA and SA culture media (T = 298 K at 50 rpm in darkness).

are widely distributed around the world and have become a serious health risk as they generate toxic metabolites that put at risk the integrity of humans, animals, and plants.[13] This microorganism can attack the carnation flower (*Dianthus caryophyllus*), a very important species in floriculture around the world. Only for Valentine's Day, nearly 600 million stems were exported worldwide. Colombia is the second producer of flowers in the world with a 16% share in the world market, and its main consumer is the United States, with a market share of approximately 78%. The control of plant pathogens present in different crops is a strategic issue. This control can be carried out by chemical, biological, and physical methods.[14,15] However, these methods are not completely effective and present side effects to plants and the environment. Heterogeneous photocatalysis is an environmentally safe and low-cost alternative against phytopathogens. Previous studies have demonstrated that semiconductors have the ability to eliminate or inactivate pathogenic microorganisms.[16−20] The effectiveness of heterogeneous photocatalysis relies on the semiconductor excitation using electromagnetic radiation to produce. The electron−hole pairs can react producing reactive oxygen species (ROS) (e.g., $OH^{\bullet}$, $O_2^{-\bullet}$). Finally, ROS can react with different molecules and destroy them.[21] Currently in the area of photocatalysis, TiO_2 is one of the most studied semiconductors due to its photocatalytic activity and high chemical and physical photostability. Furthermore, TiO_2 is considered harmless to the environment.[22,23] ZnO is another semiconductor commonly implemented in heterogeneous photocatalytic systems.[24,25] Both of them (TiO_2 and ZnO) are photocatalytically active only under UV irradiation due to their high band gap value. Various strategies have been implemented to improve photocatalytic activity (e.g., doping,[26,27] sensitization,[28,29] quantum dots,[30,31] heterostructures with other semiconductors with smaller band gap,[32,33] and anion vacancies[34]). The heterostructures have the advantage that can improve the photocatalytic activity and reduce the charge recombination rates.[35,36] Also, Rajkumar et al. reported that ZnO nanoparticles show activity against Bacillus sp., *Escherichia coli*, *Staphylococcus aureus*, *Vibrio cholerae*, Corynebacterum sp., and Salmonella sp., and the bacterial deactivation was associated with destruction of cellular walls by actions of the reactive oxygen spices (ROS).[37] In the case of TiO_2, the activity against *P. aeruginosa* PAO1 strain was reported by Kubacka et al.[38] As traditional treatments for phytopathogens are toxic to the environment and put at risk the health of the direct handler, it is necessary to look for a chemically inert alternative reduction of contaminants method that is mechanically stable and highly durable. Heterogeneous photocatalysis is an environmentally safe and low-cost alternative against phytopathogens. With this aim, in this work, we study the antimicrobial capacity of TiO_2/ZnO against FOFspd under UV irradiation. Furthermore, density functional theory (DFT) and time-dependent DFT (TDDFT) calculations were performed to support the experimental results.

2. MATERIALS AND METHODS

2.1. Thin Film: Synthesis and Characterization. Degussa powder (P25) was used as a source of TiO_2; 20 g of TiO_2 was mixed with 30 mL of isopropanol, 50 mL of distilled water, and 10 g of poly(ethylene glycol) (PEG) 1000. The obtained slurry was stirred for 20 min at 1000 rpm until suspension stabilization. Afterward, a thin film was deposited by spin coating.[39] The thin films were sintered at 500 °C. The ZnO thin films were deposited by plasma-assisted reactive evaporation technique as previously reported.[40] The structural properties of the thin films were determined by X-ray diffraction measurements and scanning electron microscopy (SEM) assays.

2.2. FOFspd Culture. The culture medium and growing conditions were performed according to the following procedure: (i) 70 mL of Sabouraud broth (0.5 cm × 1/2 cm) with fungus is brood at 25 °C for 15 days at 50 rpm. (ii) We used a sterile SEFAR PCF nylon mesh (pore diameter = 22 μm; brand SEFAR, Switzerland) to filter the spore. (iii) We concentrated the spore solution by centrifugation at 4000 rpm for 5 min. (iv) The solid was suspended in Sabouraud broth. (v) The spore counting was carried out in a Neubauer camera (2.5×10^6 spore/mL). Figure S1 shows the process of collection and counting of FOFspd spores. During the study, a strain of FOFspd was collected in Sabouraud agar (SA) and potato dextrose agar (PDA). Figure 1 shows the FOFspd in the two-culture medium.

2.3. Kinetic Adsorption Study. Before the photocatalytic process to remove a pollutant from aqueous samples begins, the adsorption/desorption equilibrium must be reached. Conventionally, before starting the photocatalytic process, the sample and the photocatalyst are stirred under conditions of darkness for 1 h. However, in this hour, it is possible to determine the potential mechanism of the kinetic adsorption process. We introduced an methylene blue (MB) solution with a concentration of 30 mg/L in a batch reactor under conditions of darkness. An aliquot was extracted at time zero and every 5 min thereafter to track the kinetics of the process. The MB concentration of each aliquot was determined by a spectrophotometer at 665 nm. We apply three models to study the MB adsorption on both thin film materials. We used the pseudo-first, pseudo-second-order, and intraparticle diffusion models to fit the kinetic results. Details of the three models can be found in Section S1 of the Supporting Information.

2.4. Photocatalytic and Inactivation Study. As a reference, we used MB as a pollutant model because it is commonly used as a standard to compare photocatalytic results

https://doi.org/10.1021/acsomega.4c01287
ACS Omega 2024, 9, 31546−31555

between different photocatalysts.[41] Although it is applied in medicine, MB represents a hazard for humans. The MB side effects include confusion, shortness of breath, red blood cell breakdown, and allergic reactions, among others.[42] We study the MB photocatalytic degradation and the activity of microorganism loss using thin films separately. Thus, the compounds were immersed in an MB aqueous solution (10 mg/L) inside the reactor, as shown in Figure 2. The UV-LED

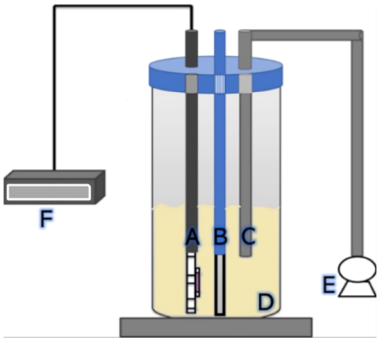

Figure 2. Reactor configuration. A: UV-LED. B: Thin film. C: Input air was pumped to the reactor. D: Spore suspension. E: Air pump. F: DC adapter LED.

lamp with an emission maximum of 260 nm and 3 W pawer was used for 250 min. The photocatalytic degradation was followed by spectrophotometry at 665 nm and the microorganism activity loss by microscopy (Neubauer camera). In the microorganism activity study, the compounds were immersed in an aqueous solution of spores (2.5×10^6 spore/mL). Again, The UV-LED lamp with an emission maximum of 260 nm and 3 W power was used for 250 min. The obtained spore counting was carried out with a Neubauer camera.

2.5. DFT Study. Density functional theory (DFT) calculations were carried out with the Amsterdam Density Functional package (ADF 2019.01)[43] using the zeroth order regular approximation Hamiltonian (ZORA) including scalar corrections.[43,44] Single polarized uncontracted type IV basis sets using triple-ζ accuracy sets of slater-type orbitals were employed.[45] The generalized gradient approximation Perdew–Burke–Ernzerhof (PBE) functional with nonlocal exchange and correlation corrections was used for the optimizations.[46] Conductor-like Screening Model (COSMO) to simulate the solvent was used, considering water as solvent.[47] A time-dependent DFT (TDDFT) method[48,49] was used to simulate the optical properties (absorption) of all compounds, using the same level of theory as the geometry optimization procedure.

3. RESULTS AND DISCUSSION

3.1. Structural Characterization. Figure 3 shows the powder X-ray pattern of the TiO_2 and ZnO thin films. TiO_2 was polycrystalline in nature. Peaks located at 2θ = 27.9 and 56.9° correspond to planes (110) and (220) of the rutile structure (JCPDS #021-1276), respectively. Furthermore, peaks located at 2θ = 25.51 and 48.31° are assigned to planes (101) and (200) in the anatase structure (JCPDS #021-1272), respectively. Using the Scherrer equation,[50,51] average crystalline size of TiO_2 was estimated to be around 19 nm using plane (101) for the anatase phase and 66 nm using plane (110) for the rutile phase. This result is according to the precursor used as the TiO_2 source. Figure 3 shows a

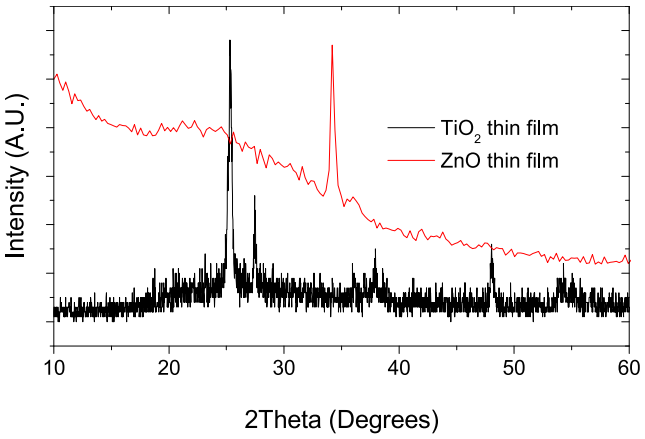

Figure 3. Powder X-ray pattern for TiO_2 and ZnO thin films.

preferential orientation plane for the ZnO thin films deposited by plasma-assisted reactive evaporation. The peaks located at 2θ = 34.41 and 36.28° correspond to the crystalline planes (002) and (101) in ZnO with hexagonal würzite crystalline phase (JCPDS #036-1451), respectively. Using the Scherrer equation, the ZnO average crystalline size was estimated to be around 32 nm using the plane (002). The powder X-ray pattern for TiO_2/ZnO thin films only shows signals corresponding to TiO_2. However, the presence of ZnO on these thin films was supported by an energy dispersive X-ray (EDX) assay (see the next section).

3.2. Morphological Characterization. Figure 4 shows the SEM images of TiO_2 and TiO_2/ZnO thin films obtained in this study. The results show that the thin films were heterogeneous, porous, and composed of different sizes of microaggregates. After ZnO was supported onto TiO_2 thin films, the ZnO particles were not distinguished. However, the presence of ZnO particles was supported by the EDX assay. Thin films show spherical particle sizes (50–200 nm). This characteristic in the morphology and particle size is typical of TiO_2 deposited from slurry suspensions (e.g., Doctor-blade and spin-coating techniques).[52,53] The final morphological properties of thin films rely on the thin film deposition experimental conditions.[54] We supported the presence of ZnO particles on the TiO_2 surface by the EDX assay. Figure 5 shows the EDX spectrum of the TiO_2/ZnO thin films. The EDX assay indicated an atomic composition of Ti (25.01%), Zn (4.44%), and O (70.54%). Despite the X-ray diffraction pattern not showing signals to ZnO for the TiO_2/ZnO thin films, Figure 5 supports the fact that ZnO was deposited on TiO_2 thin films after plasma-assisted reactive deposition.

3.3. Kinetic Study. Adsorption of the pollutant on the catalyst's surface is a previous requirement of the photocatalytic process. Figure 6 shows the fitting of three different kinetic models, and Table 1 lists the results of those fittings. The bare TiO_2 shows a removal capacity of 10.8 mg/g and TiO_2/ZnO shows a value of 12.3 mg/g. After the deposition of ZnO onto the TiO_2 surface, the catalyst shows an increment in the MB adsorption amount. This behavior can be explained by the changes in the chemical and physical properties of the surface. The TiO_2 surface was more heterogeneous after the ZnO particle modification, which assists the MB water remotion. Of the three kinetic models, the pseudo-second-order model had the best fitting results (see Table 1). This model has been reported before to describe the remotion of

https://doi.org/10.1021/acsomega.4c01287
ACS Omega 2024, 9, 31546–31555

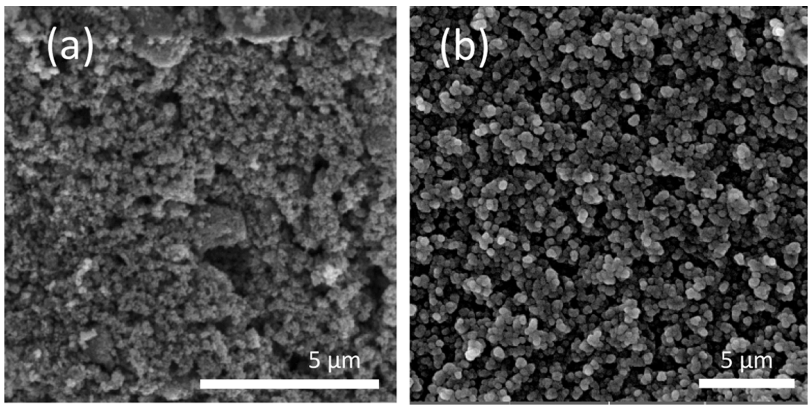

Figure 4. SEM images of (a) TiO_2 thin films and (b) TiO_2/ZnO thin films. SEM HV: 20.0 kV.

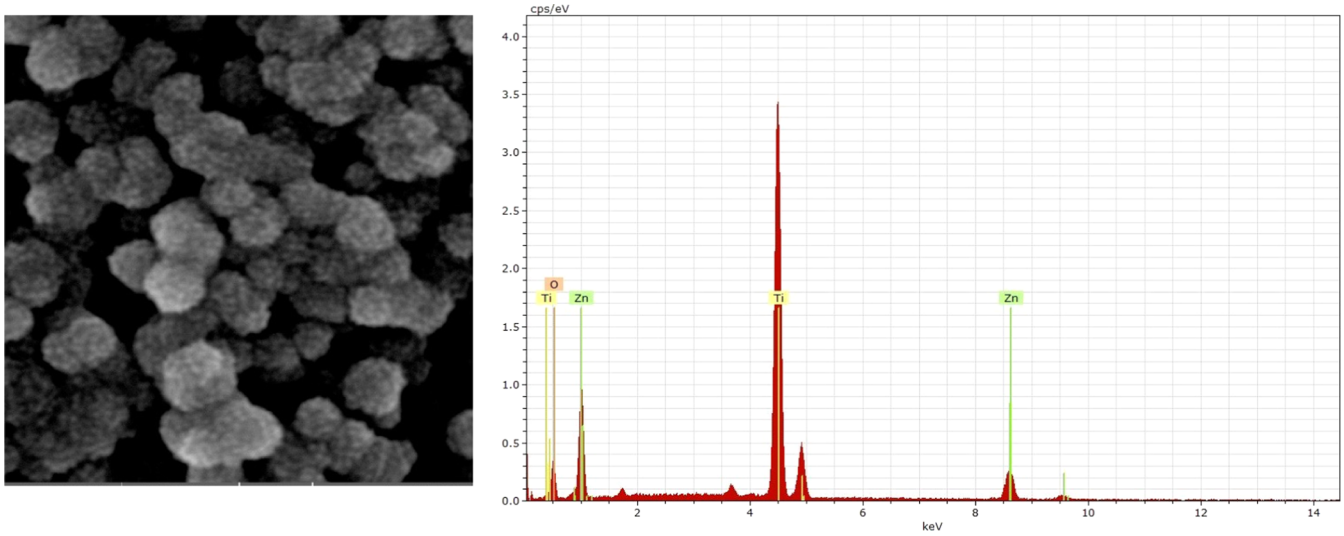

Figure 5. EDX spectrum of TiO_2/ZnO thin films. SEM HV: 20.0 kV.

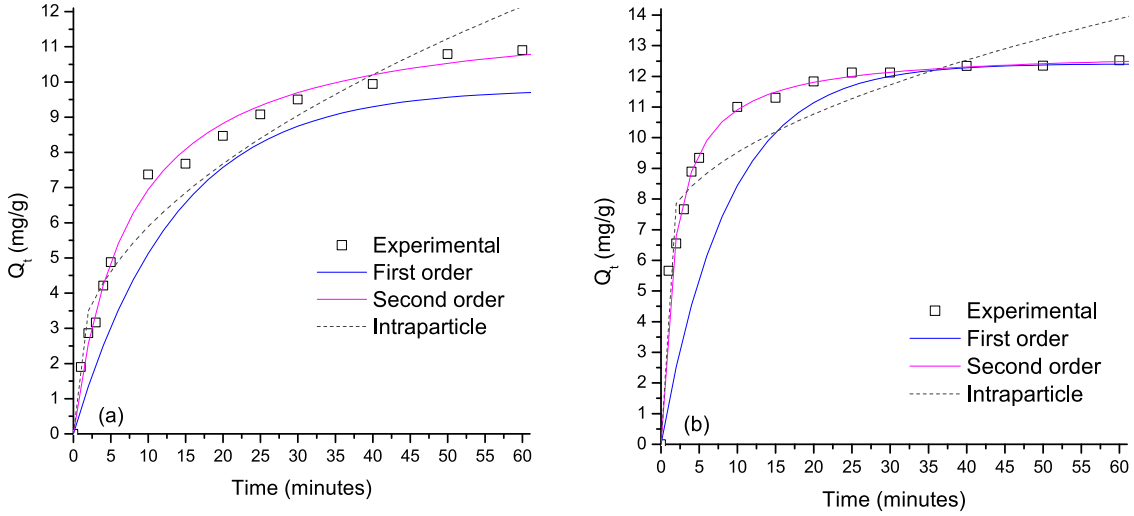

Figure 6. Fitting results for the kinetic models applied to the data of MB adsorption on (a) TiO_2 and (b) TiO_2/ZnO thin films (catalyst dosage = 0.1 g/L; stirring rate = 150 rpm, temperature = 298 K, pH= 7.0).

many compounds on different catalysts.[55,56] In this model, the electrostatic interaction is the main chemical interaction between sorbent and adsorbate during the adsorption process. MB is a typical cationic dye; thus, the MB adsorption will be favored if the charge of the semiconductor surface is negative. The isoelectric point of TiO_2 (Degussa P25) is 6.0.[57] If the pH of the solution is higher than 6.0 (we employed pH = 7.0), the cation adsorption is assisted because the surface of the catalyst is negatively charged.[58] According to the kinetic results, the electrostatic interactions (chemisorption) are present during

https://doi.org/10.1021/acsomega.4c01287
ACS Omega 2024, 9, 31546−31555

Table 1. Fitting Results for the Kinetic Adsorption Models

model fitting	parameters	TiO_2	TiO_2/ZnO
1st order	q_e (mg/g)	9.81	12.4
	k_1 (min^{-1}) × 10^{-3}	74	114
	R^2	0.938	0.927
	ARE (%)	9.4	8.2
2nd order	q_e (mg/g)	12.0	12.9
	k_2 (g/mg/min) × 10^{-3}	130	140
	R^2	0.997	0.999
	ARE (%)	5.1	2.4
intraparticle diffusion	C (mg/g)	1.57	6.51
	k_{id} (g/mg/$min^{1/2}$)	1.37	0.952
	R^2	0.933	0.798
	ARE (%)	12.8	9.5

the adsorption of MB on the catalysts. Furthermore, it is possible that this is the dominant interaction during the adsorption process. For the heterostructure TiO_2/ZnO, see Figure 6, a synergic effect in the adsorption capacity of MB is observed. This result could be explained by the changes in the morphology after the deposition of ZnO onto TiO_2 thin films.

3.4. Thin Film Photocatalytic Activity. Before testing the antimicrobial activity against FOFspd, it was decided to study the photocatalytic activity of the catalysts under UV irradiation. Figure 7(a) shows the effect of UV irradiation time on the thin film photocatalytic activity used in this study. It is observed that after 60 min of UV irradiation, the TiO_2 thin films reached 10.9% of MB degradation, whereas the TiO_2/ZnO thin films reached 20.6%. This behavior can be associated with (i) the change in the morphological properties of the thin films and (ii) the presence of heterojunction between ZnO and TiO_2 might reduce the charge carrier recombination process after UV irradiation on the semiconductor surface. The difference between the redox potential of the TiO_2 and ZnO conduction bands (CB) might assist the charge carrier separation. Even though TiO_2 and ZnO have similar energy band gap values, the CB of ZnO is located more positively than the CB of TiO_2, thus after UV irradiation a photogenerated electron can be injected from the CB_{ZnO} into the CB_{TiO_2} reducing the possibility of a recombination process.[59] We applied the Langmuir−Hinshelwood kinetic model to determine the kinetic parameters according to

$$\ln\frac{[MB]_t}{[MB]_0} = -kt \quad (1)$$

where k is the kinetic constant rate of the process and t is the time of irradiation. From this linear equation, we determined the k value for each test. Results show a $k = 1.0 \times 10^{-3}$ min^{-1} for TiO_2 and $k = 3.9 \times 10^{-3}$ min^{-1} for TiO_2/ZnO (see Figure S2 in the Supporting Information). After the modification, the photocatalytic rate was 3.9 times faster than for bare TiO_2 thin films. Both morphological and heterojunction formation might explain this increment in the photocatalytic efficiency. The TiO_2/ZnO heterojunction acts as a scavenger of the semiconductor photogenerated electrons. This property reduces the recombination process and besides, the photogenerated electron might generate ROS.[60,61] The stability of the catalyst is an important parameter in developing practical applications. In this case, we carried out 4 consecutive photocatalytic cycles with the same thin films. Figure 7(b) shows the results of the recyclability tests. Both thin films were active after 4 photocatalytic tests, and the photocatalytic efficiency was reduced by fewer than 3% in both cases. This result is associated with the great stability of the metal oxide compounds (e.g., thermal, physical, and chemical).[62,63] Furthermore, the compounds were deposited (as thin films) on a soda-lime glass substrate, which is a rigid surface with extreme physical and chemical stability.

3.5. Antimicrobial Activity against FOFspd. Monitoring the concentration of FOFsdp by microscopic observation and using the Neubauer chamber allowed us to determine the decrease in concentration over time. Also the appearance of cellular material residues from the spores destruction due to the generated ROS. Both effects are attributed to the photocatalytic process. The cell destruction causes initially deterioration in the cell wall and later in the cytoplasmic membrane. Figure 8 shows photographic evidence of FOFspd deterioration after UV irradiation over the thin films. This figure shows the loss of cell integrity and decrease in spore concentration caused by photocatalytic treatment over time.

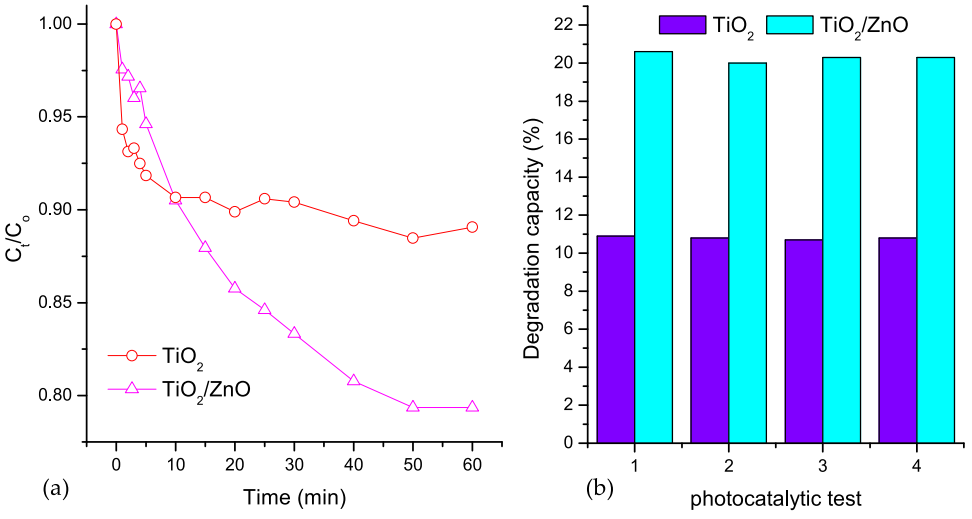

Figure 7. (a) Thin film photocatalytic activity under UV irradiation. (b) Stability test of thin films after 4 photocatalytic cycles (catalyst dosage = 0.1 g/L; stirring rate = 150 rpm, temperature = 298 K, pH = 7.0).

https://doi.org/10.1021/acsomega.4c01287
ACS Omega 2024, 9, 31546−31555

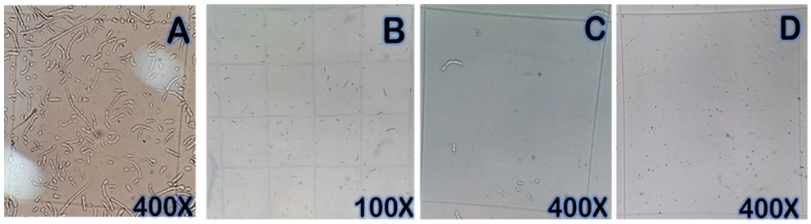

Figure 8. (A) Initial spore count (0 min of treatment), (B, C) 50 min of treatment, and (D) 250 min of treatment using TiO_2/ZnO films under UV irradiation.

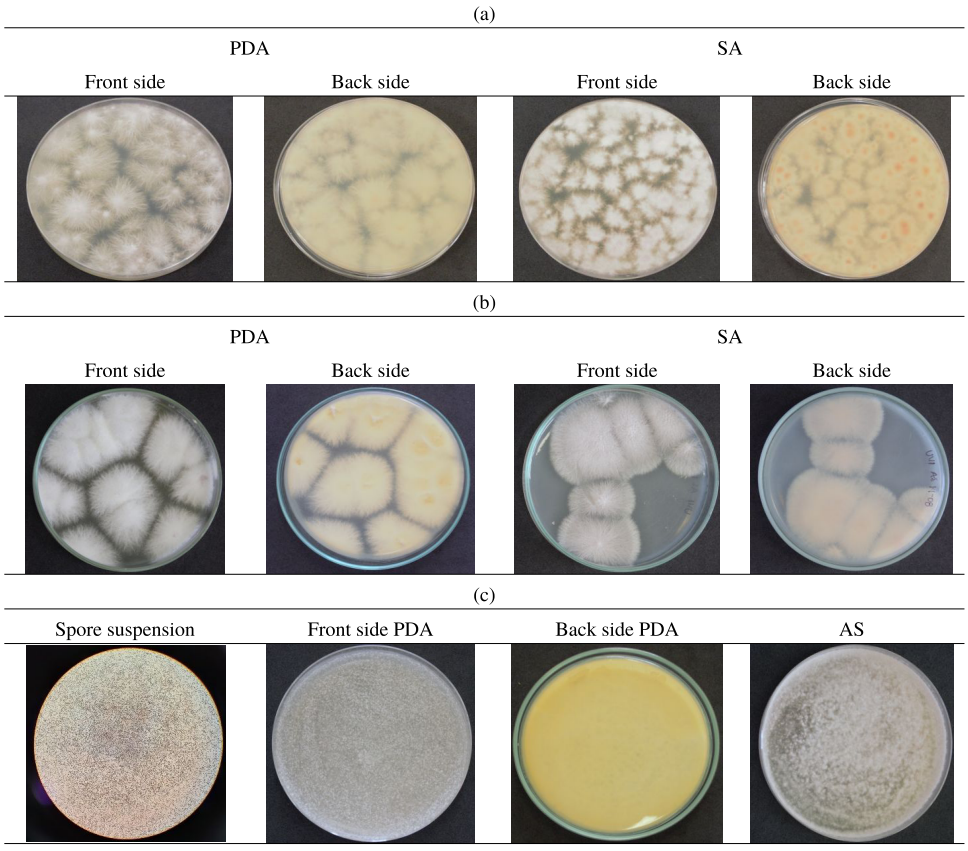

Figure 9. Culture of FOFsdp after photocatalytic treatment: (a) TiO_2 thin films, (b) TiO_2/ZnO thin films. (c) Negative control: spore without treatment.

The thin film effect is evidenced by the low number of spores per quadrant (Figure 8C,D) and by the presence of cellular material remains. The photocatalytic treatment effect was determined by the culture of the FOFsdp fungi in PDA and SA media after being irradiated with UV radiation over the catalysts. One mL of the FOFsdp suspension (2.6×10^6 spore/mL) of these treated spores was incubated in PDA and SA. After 5 days of incubation at 25 °C, we determined the fungal growth. Figure 9 shows FOFsdp growth slowly after photocatalytic treatment. Results showed isolated fungus colony growth for the samples after the photocatalytic treatment. The untreated spore (negative control) showed uniform growth (Figure 9c). This result indicates that the photocatalytic treatment affected the viability of the spores, reducing the capacity of the fungi to grow. The spore treated under UV irradiation onto TiO_2 thin films showed greater growth than the spore treated with TiO_2/ZnO thin films. The heterojunction between ZnO and TiO_2 might reduce the recombination,[64] improving the antimicrobial activity of the catalyst.

Figure 10(a) shows the normalized spore concentration FOFspd as a function of time irradiation with UV light. The TiO_2 thin films reached a reduction of 67.5% in the spore concentration of FOFspd while the TiO_2/ZnO reached a reduction of 90.1% after 250 min of UV irradiation. Two aspects can explain this behavior: (i) both semiconductors might generate ROS contributing to inactivate the FOFspd growth and (ii) the heterojunction might act as a photogenerated electron scavenger assisting the charge separation, reducing the recombination process. This charge carriers' transfer has been previously reported for other heterojunctions.[65] Figure 10(b) shows the proposed energy scheme of the heterojunction.

3.6. DFT Results. To further understand the optical properties shown by the studied materials (isolated and mixed), DFT and TDDFT calculations were performed over a reduced representation of the system. Thus, as shown in Figure

https://doi.org/10.1021/acsomega.4c01287
ACS Omega 2024, 9, 31546−31555

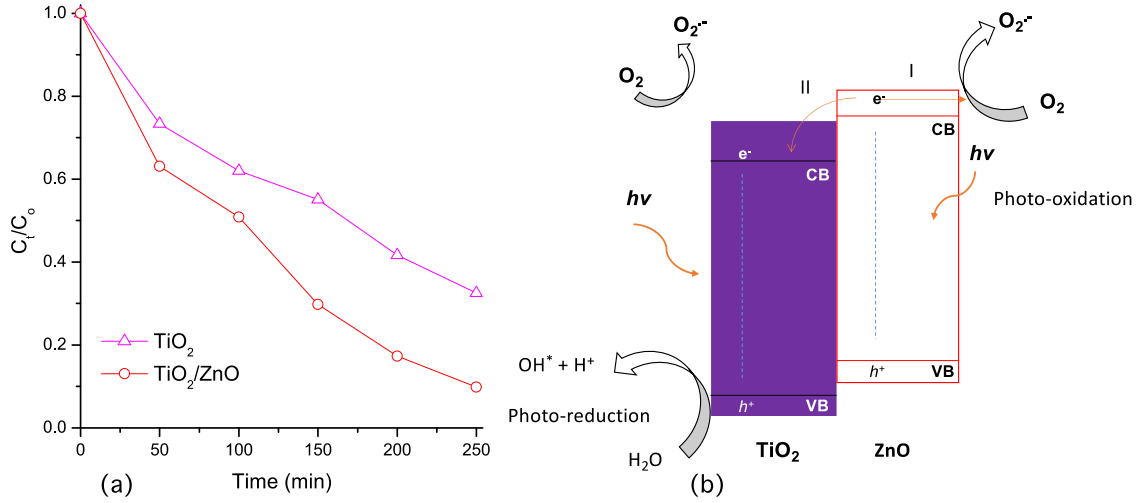

Figure 10. (a) Antimicrobial activity of materials against FOFspd. (b) Energy level of the TiO_2/ZnO heterojunction: (I) generation of reactive oxygen species by ZnO; (II) electron injection from the CB of ZnO to the CB of TiO_2.

11, the isolated nanoparticles show a geometrical structure similar to that of the mixture of the materials. In the mixed

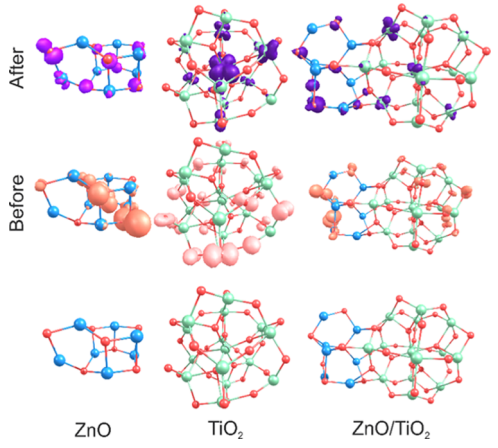

Figure 11. EDDM and the geometrical structure of the studied nanoparticles.

nanoparticle case, the M−O distances get slightly larger in the case of ZnO, whereas they turn slightly shorter in the case of TiO_2. This might be due to the electron donation from TiO_2 to ZnO, which would explain the photoinjection from ZnO to TiO_2 and the improvement in the photocatalytic and antimicrobial activity. Thus, to further understand the antimicrobial activity mechanism, TDDFT calculations were performed over the mixed TiO_2/ZnO structure. Furthermore, the electron density difference map (EDDM) isosurfaces were plotted to perform a representation of the electron density modification upon the transition, see Figure 11. As observed, the EDDM shows the occupied MOs that are depopulated and the unoccupied MOs that are populated due to the studied transition. This charge separation would explain the antimicrobial activity shown by the materials. As shown in every case, the transitions start from the oxygen atoms of the nanoparticles toward the d orbitals of the Ti atoms (when this atom is present). In the case of the pure Zn nanoparticle, most of the transition involves pi orbitals of the oxygen atoms, see Table 2. Finally, the reactivity indexes of the three studied models were calculated, see Table 3. The highest occupied

Table 2. Calculated Excitation Energies in nm, Active Molecular Orbitals (MO) and Their Contributions in %

compound	l_{Th}	f	contribution		%
TiO_2	376	0.436	p_O	d_{Ti}	100
ZnO	364	0.046	p_O	p_O	86
			p_O	p_{Zn}	14
TiO_2/ZnO	395	0.022	p_O	d_{Ti}	42
			p_O	p_O	40
			p_O	p_{Zn}	18

Table 3. DFT Results for Reactivity Indicators Calculated for the Optimized Ground State Minima of the Metallic Complexes

	HOMO	LUMO	GAP	m^a	h^b	w^c
TiO_2	−7.46	−3.94	3.52	−5.70	1.76	9.24
ZnO	−5.51	−2.23	3.27	−3.87	1.64	4.57
TiO_2/ZnO	−6.71	−3.83	2.87	−5.27	1.44	9.67

[a]Chemical potential. [b]Chemical hardness. [c]Electrophilicity.

molecular orbital−lowest unoccupied molecular orbital (HOMO−LUMO) GAP decreases for the mixed nanoparticle system, showing its increased reactivity. Furthermore, the chemical hardness shows its lower value for the mixed system and also the electrophilicity index has its largest value, supporting the larger reactivity for the mixed nanoparticle system.

4. CONCLUSIONS

In this study, the antimicrobial activity of TiO_2/ZnO against FOFsdp was studied. Furthermore, the removal efficiency and the photocatalytic degradation study of MB were performed. TiO_2/ZnO was more efficient in the MB removal from an aqueous solution than bare TiO_2. Furthermore, the TiO_2/ZnO thin films were more efficient in reducing the spore concentration (90.1%) against FOFsdp than against bare TiO2 (67.5%). By means of TDDFT calculations, it was shown a mixed participation of both portions of the mixed nanoparticles. Furthermore, the large reactivity observed for the mixed nanoparticle can be attributed to the diminution in the HOMO−LUMO GAP and increased reactivity indexes.

https://doi.org/10.1021/acsomega.4c01287
ACS Omega 2024, 9, 31546−31555

Finally, the mixture of ZnO with TiO_2 increases its biological activity against FOFspd, showing that the materials studied herein could be a great and cheap alternative for fungal treatments.

■ ASSOCIATED CONTENT

Supporting Information

The Supporting Information is available free of charge at https://pubs.acs.org/doi/10.1021/acsomega.4c01287.

Process of collection and counting of *Fusarium oxysporum* f. sp. dianthi (Figure S1); Langmuir−Hinshelwood fitting model of kinetical results shown in Figure 10 (Figure S1); kinetic study models (Section S1) (PDF)

■ AUTHOR INFORMATION

Corresponding Author

William Vallejo − *Grupo de Fotoquímica y Fotobiología, Universidad del Atlántico, Puerto Colombia 81007, Colombia;* orcid.org/0000-0002-6661-545X; Phone: +57-6053599484; Email: williamvallejo@mail.uniatlantico.edu.co

Authors

Cesar Quiñones − *Facultad de ingeniería, Programa de ingeniería Química, Universidad de La Salle, Bogotá 111711, Colombia*

Martha Posada − *Grupo de Investigación Ceparium, Universidad Colegio Mayor de Cundinamarca, Bogotá 111321, Colombia*

Angie Hormiga − *Grupo de Investigación Ceparium, Universidad Colegio Mayor de Cundinamarca, Bogotá 111321, Colombia*

Julian Peña − *Escuela de negocios, Universidad del Caribe (UNICARIBE), Santo Domingo 11105, República Dominicana*

Carlos Diaz-Uribe − *Grupo de Fotoquímica y Fotobiología, Universidad del Atlántico, Puerto Colombia 81007, Colombia*

Amner Muñoz-Acevedo − *Grupo de Investigación en Química y Biología, Universidad del Norte, Puerto Colombia 81007, Colombia*

Vanesa Roa − *Departamento de Química Inorgánica, Facultad de Química y Farmacia, Centro de Energía UC, Centro de Investigación en Nanotecnología y Materiales Avanzados CIEN-UC, Pontificia Universidad Católica de Chile, 4860 Santiago, Chile*

Eduardo Schott − *Departamento de Química Inorgánica, Facultad de Química y Farmacia, Centro de Energía UC, Centro de Investigación en Nanotecnología y Materiales Avanzados CIEN-UC, Pontificia Universidad Católica de Chile, 4860 Santiago, Chile*

Ximena Zarate − *Instituto de Ciencias Aplicadas, Facultad de Ingeniería, Universidad Autónoma de Chile, Santiago 7500912, Chile*

Complete contact information is available at: https://pubs.acs.org/10.1021/acsomega.4c01287

Notes

The authors declare no competing financial interest.

■ ACKNOWLEDGMENTS

W.V. and C.D.-U. thank Universidad del Atlántico. E.S. and X.Z. gratefully acknowledge FONDECYT 1241917, 1231194, and ANID/FONDAP/1523A0006. ACT210057. A.M.-A. thanks the Vicerrectoría de Investigaciones of the Universidad del Norte for the financial support for the article processing charge.

■ REFERENCES

(1) Priyadarshini, M.; Das, I.; Ghangrekar, M. M.; Blaney, L. Advanced Oxidation Processes: Performance, Advantages, and Scale-up of Emerging Technologies. *J. Environ. Manage.* **2022**, *316*, No. 115295.

(2) Ejhieh, A. N.; Khorsandi, M. Photodecolorization of Eriochrome Black T Using NiS−P Zeolite as a Heterogeneous Catalyst. *J. Hazard. Mater.* **2010**, *176* (1−3), 629−637.

(3) Dell'Edera, M.; Lo Porto, C.; De Pasquale, I.; Petronella, F.; Curri, M. L.; Agostiano, A.; Comparelli, R. Photocatalytic TiO2-Based Coatings for Environmental Applications. *Catal. Today* **2021**, *380*, 62−83.

(4) Sharma, M.; Yadav, A.; Mandal, M. K.; Dubey, K. K. TiO2 Based Photocatalysis: A Valuable Approach for the Removal of Pharmaceuticals from Aquatic Environment. *Int. J. Environ. Sci. Technol.* **2023**, *20* (4), 4569−4584.

(5) Wang, H.; Li, X.; Zhao, X.; Li, C.; Song, X.; Zhang, P.; Huo, P.; Li, X. A Review on Heterogeneous Photocatalysis for Environmental Remediation: From Semiconductors to Modification Strategies. *Chin. J. Catal.* **2022**, *43* (2), 178−214.

(6) Hemmatpour, P.; Nezamzadeh-Ejhieh, A. A Z-Scheme CdS/BiVO4 Photocatalysis towards Eriochrome Black T: An Experimental Design and Mechanism Study. *Chemosphere* **2022**, *307* (Pt 2), No. 135925.

(7) Mirian, Z. A.; Nezamzadeh-Ejhieh, A. Removal of Phenol Content of an Industrial Wastewater via a Heterogeneous Photodegradation Process Using Supported FeO onto Nanoparticles of Iranian Clinoptilolite. *Desalin. Water Treat.* **2016**, *57* (35), 16483−16494.

(8) Iazdani, F.; Nezamzadeh-Ejhieh, A. Photocatalytic Kinetics of 2,4-Dichloroaniline Degradation by NiO-Clinoptilolite Nanoparticles. *Spectrochim. Acta, Part A* **2021**, *250*, No. 119228.

(9) Rahmani-Aliabadi, A.; Nezamzadeh-Ejhieh, A. A Visible Light FeS/Fe2S3/Zeolite Photocatalyst towards Photodegradation of Ciprofloxacin. *J. Photochem. Photobiol., A* **2018**, *357*, 1−10.

(10) Durgalakshmi, D.; Ajay Rakkesh, R.; Rajendran, S.; Naushad, M. Principles and Mechanisms of Green Photocatalysis. In *Green Photocatalysts*; Springer: Cham, 2020; pp 1−24.

(11) Cavicchioli, R.; Ripple, W. J.; Timmis, K. N.; Azam, F.; Bakken, L. R.; Baylis, M.; Behrenfeld, M. J.; Boetius, A.; Boyd, P. W.; Classen, A. T.; Crowther, T. W.; Danovaro, R.; Foreman, C. M.; Huisman, J.; Hutchins, D. A.; Jansson, J. K.; Karl, D. M.; Koskella, B.; Mark Welch, D. B.; Martiny, J. B. H.; Moran, M. A.; Orphan, V. J.; Reay, D. S.; Remais, J. V.; Rich, V. I.; Singh, B. K.; Stein, L. Y.; Stewart, F. J.; Sullivan, M. B.; van Oppen, M. J. H.; Weaver, S. C.; Webb, E. A.; Webster, N. S. Scientists' Warning to Humanity: Microorganisms and Climate Change. *Nat. Rev. Microbiol.* **2019**, *17* (9), 569−586.

(12) Miller, S. A.; Ferreira, J. P.; Lejeune, J. T. Antimicrobial Use and Resistance in Plant Agriculture: A One Health Perspective. *Agriculture* **2022**, *12* (2), No. 289.

(13) Ardila, H. D.; Torres, A. M.; Martínez, S. T.; Higuera, B. L. Biochemical and Molecular Evidence for the Role of Class III Peroxidases in the Resistance of Carnation (Dianthus Caryophyllus L) to Fusarium Oxysporum f. Sp. Dianthi. *Physiol. Mol. Plant Pathol.* **2014**, *85*, 42−52.

(14) Tariq, M.; Khan, A.; Asif, M.; Khan, F.; Ansari, T.; Shariq, M.; Siddiqui, M. A. Biological Control: A Sustainable and Practical Approach for Plant Disease Management. *Acta Agric. Scand., Sect. B* **2020**, *70*, 507−524.

(15) Borges, D. F.; Lopes, E. A.; Fialho Moraes, A. R.; Soares, M. S.; Visôtto, L. E.; Oliveira, C. R.; Moreira Valente, V. M. Formulation of Botanicals for the Control of Plant-Pathogens: A Review. *Crop Prot.* **2018**, *110*, 135−140.
(16) Saravanan, A.; Kumar, P. S.; Jeevanantham, S.; Karishma, S.; Kiruthika, A. R. Photocatalytic Disinfection of Micro-Organisms: Mechanisms and Applications. *Environ. Technol. Innovation* **2021**, *24*, No. 101909.
(17) Skwor, T. A.; Klemm, S.; Zhang, H.; Schardt, B.; Blaszczyk, S.; Bork, M. A. Photodynamic Inactivation of Methicillin-Resistant Staphylococcus Aureus and *Escherichia Coli*: A Metalloporphyrin Comparison. *J. Photochem. Photobiol., B* **2016**, *165*, 51−57.
(18) Shimizu, Y.; Ateia, M.; Wang, M.; Awfa, D.; Yoshimura, C. Disinfection Mechanism of *E. Coli* by CNT-TiO2 Composites: Photocatalytic Inactivation vs. Physical Separation. *Chemosphere* **2019**, *235*, 1041−1049.
(19) Nyangaresi, P. O.; Qin, Y.; Chen, G.; Zhang, B.; Lu, Y.; Shen, L. Comparison of UV-LED Photolytic and UV-LED/TiO2 Photocatalytic Disinfection for *Escherichia Coli* in Water. *Catal. Today* **2019**, *335*, 200−207.
(20) De Pasquale, I.; Porto, C. L.; Dell'Edera, M.; Petronella, F.; Agostiano, A.; Curri, M. L.; Comparelli, R. Photocatalytic TiO2-Based Nanostructured Materials for Microbial Inactivation. *Catalysis* **2020**, *10* (12), No. 1382.
(21) Shams-Ghahfarokhi, Z.; Nezamzadeh-Ejhieh, A. As-Synthesized ZSM-5 Zeolite as a Suitable Support for Increasing the Photoactivity of Semiconductors in a Typical Photodegradation Process. *Mater. Sci. Semicond. Process.* **2015**, *39*, 265−275.
(22) Guo, Q.; Zhou, C.; Ma, Z.; Yang, X. Fundamentals of TiO 2 Photocatalysis: Concepts, Mechanisms, and Challenges. *Adv. Mater.* **2019**, *31* (50), No. 1901997.
(23) Anucha, C. B.; Altin, I.; Bacaksiz, E.; Stathopoulos, V. N. Titanium Dioxide (TiO_2)-Based Photocatalyst Materials Activity Enhancement for Contaminants of Emerging Concern (CECs) Degradation: In the Light of Modification Strategies. *Chem. Eng. J. Adv.* **2022**, *10*, No. 100262.
(24) Ong, C. B.; Ng, L. Y.; Mohammad, A. W. A Review of ZnO Nanoparticles as Solar Photocatalysts: Synthesis, Mechanisms and Applications. *Renewable Sustainable Energy Rev.* **2018**, *81*, 536−551.
(25) Bharat, T. C.; Shubham; Mondal, S.; Gupta, H. S.; Singh, P. K.; Das, A. K. Synthesis of Doped Zinc Oxide Nanoparticles: A Review. In *Mater. Today: Proc.*; Elsevier Ltd., 2019; Vol. *11*, pp 767−775.
(26) Khlyustova, A.; Sirotkin, N.; Kusova, T.; Kraev, A.; Titov, V.; Agafonov, A. Doped TiO2: The Effect of Doping Elements on Photocatalytic Activity. *Mater. Adv.* **2020**, *1* (5), 1193−1201.
(27) Vallejo, W.; Cantillo, A.; Salazar, B.; Diaz-Uribe, C.; Ramos, W.; Romero, E.; Hurtado, M. Comparative Study of ZnO Thin Films Doped with Transition Metals (Cu and Co) for Methylene Blue Photodegradation under Visible Irradiation. *Catalysts* **2020**, *10* (5), No. 528.
(28) Vallejo, W.; Rueda, A.; Díaz-Uribe, C.; Grande, C.; Quintana, P. Photocatalytic Activity of Graphene Oxide−TiO2 Thin Films Sensitized by Natural Dyes Extracted from Bactris Guineensis. *R. Soc. Open Sci.* **2019**, *6* (3), No. 181824.
(29) Vo, H. T.; Nguyen, A. T.; Tran, C. V.; Nguyen, S. X.; Tung, N. T.; Pham, D. T.; Nguyen, D. D.; La, D. D. Self-Assembly of Porphyrin Nanofibers on ZnO Nanoparticles for the Enhanced Photocatalytic Performance for Organic Dye Degradation. *ACS Omega* **2021**, *6*, 23203−23210.
(30) Shalahuddin Al Ja'farawy, M.; Kusumandari; Purwanto, A.; Widiyandari, H. Carbon Quantum Dots Supported Zinc Oxide (ZnO/CQDs) Efficient Photocatalyst for Organic Pollutant Degradation − A Systematic Review. *Environ. Nanotechnol., Monit. Manage.* **2022**, *18*, No. 100681.
(31) Baragau, I. A.; Buckeridge, J.; Nguyen, K. G.; Heil, T.; Sajjad, M. T.; Thomson, S. A. J.; Rennie, A.; Morgan, D. J.; Power, N. P.; Nicolae, S. A.; Titirici, M. M.; Dunn, S.; Kellici, S. Outstanding Visible Light Photocatalysis Using Nano-TiO2 Hybrids with Nitrogen-Doped Carbon Quantum Dots and/or Reduced Graphene Oxide. *J. Mater. Chem. A* **2023**, *11* (18), 9791−9806.
(32) Qutub, N.; Singh, P.; Sabir, S.; Sagadevan, S.; Oh, W. C. Enhanced Photocatalytic Degradation of Acid Blue Dye Using CdS/TiO2 Nanocomposite. *Sci. Rep.* **2022**, *12* (1), No. 5759.
(33) Nandi, P.; Das, D. ZnO/CdS/CuS Heterostructure: A Suitable Candidate for Applications in Visible-Light Photocatalysis. *J. Phys. Chem. Solids* **2022**, *160*, No. 110344.
(34) Rezaei, M.; Nezamzadeh-Ejhieh, A.; Massah, A. R. A Comprehensive Review on the Boosted Effects of Anion Vacancy in the Heterogeneous Photocatalytic Degradation, Part II: Focus on Oxygen Vacancy. *ACS Omega* **2023**, *9* (6), 6093−6127.
(35) Mahala, C.; Sharma, M. D.; Basu, M. ZnO@CdS Heterostructures: An Efficient Photoanode for Photoelectrochemical Water Splitting. *New J. Chem.* **2019**, *43* (18), 7001−7010.
(36) Guo, X.; Liu, X.; Yan, J.; Liu, S. F. Heterointerface Engineering of ZnO/CdS Heterostructures through ZnS Layers for Photocatalytic Water Splitting. *Chem. - Eur. J.* **2022**, *28* (69), No. e202202662.
(37) Rajkumar, K. S.; Arun, S.; Dinesh Babu, M.; Balaji, P.; Sivasubramanian, S.; Vignesh, V.; Thirumurugan, R. Facile Biofabrication, Characterization, Evaluation of Photocatalytic, Antipathogenic Activity and in Vitro Cytotoxicity of Zinc Oxide Nanoparticles. *Biocatal. Agric. Biotechnol.* **2019**, *22*, No. 101436.
(38) Kubacka, A.; Diez, M. S.; Rojo, D.; Bargiela, R.; Ciordia, S.; Zapico, I.; Albar, J. P.; Barbas, C.; Santos, V. A. P. M.; dos Fernández-García, M.; Ferrer, M. Understanding the Antimicrobial Mechanism of TiO2-Based Nanocomposite Films in a Pathogenic Bacterium. *Sci. Rep.* **2014**, *4* (1), No. 4134.
(39) Kontos, A. I.; Kontos, A. G.; Tsoukleris, D. S.; Bernard, M.-C.; Spyrellis, N.; Falaras, P. Nanostructured TiO2 Films for DSSCS Prepared by Combining Doctor-Blade and Sol−Gel Techniques. *J. Mater. Process. Technol.* **2008**, *196* (1−3), 243−248.
(40) Gordillo, G.; Pena, J. C. Development of System to Grow ZnO Films by Plasma Assisted Reactive Evaporation with Improved Thickness Homogeneity for Using in Solar Cells. *J. Mater. Res. Technol.* **2022**, *19*, 1191−1202.
(41) Mills, A. An Overview of the Methylene Blue ISO Test for Assessing the Activities of Photocatalytic Films. *Appl. Catal., B* **2012**, *128*, 144−149.
(42) Mirsalari, S. A.; Nezamzadeh-Ejhieh, A. Focus on the Photocatalytic Pathway of the CdS-AgBr Nano-Catalyst by Using the Scavenging Agents. *Sep. Purif. Technol.* **2020**, *250*, No. 117235.
(43) te Velde, G.; Bickelhaupt, F. M.; Baerends, E. J.; Fonseca Guerra, C.; van Gisbergen, S. J. A.; Snijders, J. G.; Ziegler, T. Chemistry with ADF. *J. Comput. Chem.* **2001**, *22* (9), 931−967.
(44) Van Lenthe, E.; Baerends, E. J.; Snijders, J. G. Relativistic Total Energy Using Regular Approximations. *J. Chem. Phys.* **1994**, *101* (11), 9783.
(45) Snijders, J. G.; Vernooijs, P.; Baerends, E. J. Roothaan-Hartree-Fock-Slater Atomic Wave Functions: Single-Zeta, Double-Zeta, and Extended Slater-Type Basis Sets for 87 Fr-103Lr. *At. Data Nucl. Data Tables* **1981**, *26* (6), 483−509.
(46) Laskowski, R.; Blaha, P.; Tran, F. Assessment of DFT Functionals with NMR Chemical Shifts. *Phys. Rev. B* **2013**, *87* (19), No. 195130.
(47) Toure, O.; Lebert, A.; Dussap, C. G. Extension of the COSMO-RS-PDHS Model to the Prediction of Activity Coefficients in Concentrated {water-Electrolyte} and {water-Polyol} Solutions. *Fluid Phase Equilib.* **2016**, *424*, 90−104.
(48) Runge, E.; Gross, E. K. U. Density-Functional Theory for Time-Dependent Systems. *Phys. Rev. Lett.* **1984**, *52* (12), No. 997.
(49) Wang, F.; Ziegler, T.; Van Lenthe, E.; Van Gisbergen, S.; Baerends, E. J. The Calculation of Excitation Energies Based on the Relativistic Two-Component Zeroth-Order Regular Approximation and Time-Dependent Density-Functional with Full Use of Symmetry. *J. Chem. Phys.* **2005**, *122* (20), No. 204103.
(50) Derikvandi, H.; Nezamzadeh-Ejhieh, A. Increased Photocatalytic Activity of NiO and ZnO in Photodegradation of a Model

https://doi.org/10.1021/acsomega.4c01287
ACS Omega 2024, 9, 31546−31555

Drug Aqueous Solution: Effect of Coupling, Supporting, Particles Size and Calcination Temperature. *J. Hazard. Mater.* **2017**, *321*, 629−638.
(51) Zabihi-Mobarakeh, H.; Nezamzadeh-Ejhieh, A. Application of Supported TiO2 onto Iranian Clinoptilolite Nanoparticles in the Photodegradation of Mixture of Aniline and 2, 4-Dinitroaniline Aqueous Solution. *J. Ind. Eng. Chem.* **2015**, *26*, 315−321.
(52) Lukong, V. T.; Mouchou, R. T.; Enebe, G. C.; Ukoba, K.; Jen, T. C. Deposition and Characterization of Self-Cleaning TiO2 Thin Films for Photovoltaic Application. *Mater. Today Proc.* **2022**, *62*, S63−S72.
(53) Vallejo, W.; Diaz-Uribe, C.; Quiñones, C. Optical and Structural Characterization of Cd-Free Buffer Layers Fabricated by Chemical Bath Deposition. *Coatings* **2021**, *11* (8), No. 897.
(54) Budida, J.; Srinivasan, K. Review of Thin Film Deposition and Techniques. *Mater. Today Proc.* **2023**, *92*, 1030.
(55) Yagub, M. T.; Sen, T. K.; Afroze, S.; Ang, H. M. Dye and Its Removal from Aqueous Solution by Adsorption: A Review. *Adv. Colloid Interface Sci.* **2014**, *209*, 172−184.
(56) Nasiri-Ardali, M.; Nezamzadeh-Ejhieh, A. A Comprehensive Study on the Kinetics and Thermodynamic Aspects of Batch and Column Removal of Pb(II) by the Clinoptilolite−Glycine Adsorbent. *Mater. Chem. Phys.* **2020**, *240*, No. 122142.
(57) Jiang, J.; Oberdörster, G.; Biswas, P. Characterization of Size, Surface Charge, and Agglomeration State of Nanoparticle Dispersions for Toxicological Studies. *J. Nanopart. Res.* **2009**, *11* (1), 77−89.
(58) Dinh, V. P.; Xuan, T. D.; Hung, N. Q.; Luu, T. T.; Do, T. T. T.; Nguyen, T. D.; Nguyen, V. D.; Anh, T. T. K.; Tran, N. Q. Primary Biosorption Mechanism of Lead (II) and Cadmium (II) Cations from Aqueous Solution by Pomelo (Citrus Maxima) Fruit Peels. *Environ. Sci. Pollut. Res.* **2021**, *28* (45), 63504−63515.
(59) Tiwana, P.; Docampo, P.; Johnston, M. B.; Snaith, H. J.; Herz, L. M. Electron Mobility and Injection Dynamics in Mesoporous ZnO, SnO 2, and TiO2 Films Used in Dye-Sensitized Solar Cells. *ACS Nano* **2011**, *5* (6), 5158−5166.
(60) Nezamzadeh-Ejhieh, A.; Hushmandrad, S. Solar Photodecolorization of Methylene Blue by CuO/X Zeolite as a Heterogeneous Catalyst. *Appl. Catal., A* **2010**, *388* (1−2), 149−159.
(61) Karimi-Shamsabadi, M.; Nezamzadeh-Ejhieh, A. Comparative Study on the Increased Photoactivity of Coupled and Supported Manganese-Silver Oxides onto a Natural Zeolite Nano-Particles. *J. Mol. Catal. A: Chem.* **2016**, *418*−*419*, 103−114.
(62) Hosny, N. M.; Gomaa, I.; Elmahgary, M. G. Adsorption of Polluted Dyes from Water by Transition Metal Oxides: A Review. *Appl. Surf. Sci. Adv.* **2023**, *15*, No. 100395.
(63) Virt, I. Special Issue: Recent Advances in Semiconducting Thin Films. *Coatings* **2023**, *13* (1), No. 79.
(64) Shen, K.; Wu, K.; Wang, D. Band alignment of ultra-thin hetero-structure ZnO/TiO_2 junction. *Mater. Res. Bull.* **2014**, *51*, 141−144.
(65) Farsi, M.; Nezamzadeh-Ejhieh, A. A Z-Scheme Cobalt(II) Oxide-Silver Tungstate Nano Photocatalyst: Experimental Design and Mechanism Study for the Degradation of Methylene Blue. *Surf. Interfaces* **2022**, *32*, No. 102148.

https://doi.org/10.1021/acsomega.4c01287
ACS Omega 2024, 9, 31546−31555